

https://dspace.org/

Strength and durability performance of hybrid alkaline clay brick waste coconut shell ash cement

Festus Ngui; Victor Mutai; Najya Muhammed; Fredrick Mutunga; Joseph Marangu ...

https://hdl.handle.net/10539/43604
SCOPUS

Downloaded from a DSpace repository. https://dspace.org/

Journal of Sustainable Construction Materials and Technologies
Web page info: https://jscmt.yildiz.edu.tr
DOI: 10.47481/jscmt.1607846

JSCMT
Journal of Sustainable Construction Materials and Technologies

Research Article

Strength and durability performance of hybrid alkaline clay brick waste – Coconut shell ash cement

Festus Musyimi NGUI*[1], Victor Kiptoo MUTAI[2], Najya MUHAMMED[1], Fredrick Mulei MUTUNGA[1], Joseph Mwiti MARANGU[3], Mike OTIENO[4]

[1]*Department of Chemistry, Pwani University, Kilifi, Kenya*
[2]*Department of Geoscience, University of Padova, Padova, Italy*
[3]*Department of Physical Sciences, Meru University of Science and Technology, Meru, Kenya*
[4]*School of Civil and Environmental Engineering, University of the Witwatersrand, Johannesburg, South Africa*

ARTICLE INFO

Article history
Received: 04 June 2024
Revised: 27 September 2024
Accepted: 04 October 2024

Key words:
Alkali activator, clay brick waste, coconut shell ash, durability, hybrid alkaline mortar, sodium sulphate

ABSTRACT

Hybrid Alkaline Cement (HAC) has the potential to reduce carbon dioxide (CO_2) and improve concrete structure. The durability of a hybrid alkaline mortar made from a mixture of calcined clay brick waste (CBW) and coconut shell ash (CSA) was compared with that of ordinary Portland cement (OPC) and pozzolanic Portland cement (PPC), which are the two common types of Portland cement. In an open furnace, CSA was obtained by burning coconut shells collected from Kilifi County, Kenya. At the same time, CBW was sampled from brick production and construction sites in Kibwezi sub-county, Kenya, and ground using a laboratory ball mill. Various cement blends were prepared by mixing different mass ratios of OPC:CSA: CBW and activated with 0.5 M and 2 M Sodium sulfate solutions, maintaining a solution-to-cement ratio of 0.5. Control mortar prisms were cast using distilled water and cured in distilled water. Principle Component Analysis (PCA) was used for correlation analysis. Compressive strength development, water sorptivity, Porosity, oxygen permeability index, and thermal resistance were investigated for durability properties. Accelerated chloride ingress and chloride ion diffusion coefficients were determined. Results show that alkali-activated samples exhibited lower sorptivity, Porosity, chloride ingress, and higher compressive strength, oxygen permeability index, and thermal resistance than the cement mix prepared with water. The mix designs 5-1-4, 5-4-1, 3-1-6, and 3-6-1 demonstrated a decreasing optimum performance comparable to OPC in that order. The formulation 5-1-4, prepared with 2 M Sodium sulfate, showed the highest durability in all tests. Moreover, mortar durability was highly influenced by the amount of cement substituted, the kind of precursor, and the concentration of alkali activator.

Cite this article as: Ngui, F. M., Mutai, V. K., Muhammed, N., Mutunga, F. M., Marangu, J. M., & Otieno, M. (2024). Strength and durability performance of hybrid alkaline clay brick waste – Coconut shell ash cement. *J Sustain Const Mater Technol*, 9(4), 000–000.

1. INTRODUCTION

The cement manufacturing industry accounts for roughly 6–8% of global CO_2 emissions annually [1]. We must reduce CO_2 emissions from cement production to mitigate this environmental impact. Using alternative materials, mainly agricultural and industrial waste that would otherwise end up in landfills, presents a viable solution. Hybrid-activated cement (HAC) is emerging as a potential long-term substitutes for traditional Portland cement concrete (PCC) [2].

***Corresponding author.**
*E-mail address: festongu@gmail.com

Published by Yıldız Technical University Press, İstanbul, Türkiye
This is an open access article under the CC BY-NC license (http://creativecommons.org/licenses/by-nc/4.0/).

Producing such cement involves substituting the main clinker component. Replacing PCC with HAC has the potential to reduce carbon emissions by 9% to 80% [1, 3]. Several factors, including the chemistry of the alkaline activator, fuel prices, raw material availability, and the efficiency of the clinkering operation in a given region, affect the degree to which emissions can be reduced. However, the durability of the concrete structure is of great importance as CO_2 reduction is achieved.

The durability of concrete structures made with Ordinary Portland Cement (OPC) depends on the quality of the cement and raw materials used. Climate changes, acidic conditions, and carbonationally threaten concrete durability. Exposure to high temperatures causes several chemical and physical transformations in cementitious materials, resulting in internal pore pressure, different thermal expansion rates of components, and decomposition of cement compounds [4]. Once hardened, the cement paste is the least stable component. Due to the degradation of calcium hydroxide (CH) and calcium silicate hydrate (C-S-H), OPC is physically and chemically degraded at high temperatures [5].

In contrast, HAC structures exhibit resilient performance under adverse conditions. They are characterized by low CH and C-S-H content, forming a stable three-dimensional Sodium Alumino-Silicate Hydrate (N-A-S-H) gel formed by connecting SiO_4 and AlO_4 tetrahedra with O atoms in alternating cycles [6, 7]. This results in HAC blends with thermal conductivity typically less than 1 W/m.C, making them an excellent thermal insulator [8]. Aggregate Porosity and mineralogy also influence degradation severity [9]. Concrete deterioration often allows external aggressive chemicals, such as chloride ions, water, and oxygen, to penetrate the concrete matrix through pores and microscopic fissures. The main pathways for ingress into the system are permeability, capillary absorption, and diffusion [10]. Permeability, or the combination of pore structure and proportion of capillary pores, determines how well concrete resists aggressive chemicals. The binder's formulation is the most critical component that affects the permeability of concrete. Binders made from alkali-activated well-blended OPC exhibit denser microstructures than those made from the OPC system, contributing to HAC's enhanced performance potential.

Despite the long history of alkaline activation of aluminosilicates [11, 12], hybrid alkali-activated agricultural and industrial binders have only recently gained recognition as acceptable substitutes for Portland cement [13, 14]. However, the long-term durability of HAC remains to be definitively demonstrated, especially concerning properties related to aggressive ion permeability and thermal resistance.

Thus, further research is needed to enhance engineers' and concrete practitioners' understanding of HAC as an alternative to conventional concrete. This study aims to address critical challenges related to the permeability of aggressive agents and the fire resistance of novel binder construction materials. Specifically, a focus on hybrid alkaline blend materials to investigate changes in sorptivity and chloride ion permeability as OPC replacement, alkali activator concentration, and CBW: CSA ratio are adjusted. Thermal resistance is also evaluated as an essential attribute.

Table 1. Relative percentages of binder type for mortar (w/c=0.5, 28 days curing)

Binder	OPC	CSA	CBW
OPC	100	0	0
5-1-4*	50	10	40
5-4-1*	50	40	10
3-1-6*	30	10	60
3-6-1*	30	60	10

*: Label based on the mix mass ratio of PC-to-CSA-to-CBW. OPC: Ordinary portland cement; CSA: Coconut shell ash; CBW: Clay brick waste.

2. MATERIALS AND METHODS

2.1. Blaine test and Preparation of Mortar Prisms

The specific surface area of the binders was determined according to the Blaine test protocol outlined in the K S EAS 148:-6:1 (2000) standard. Mortar prisms were prepared for Testing by KS EAS 148: 1 [15] using 1,350 g of standard sand complying with EN 196. A mixture of 450 g of test cement and standard sand was prepared using a PAN Analytica mixer machine for 1 minute. Subsequently, an alkaline solution of 0.5 M or 2 M Na_2SO_4, was added to achieve the desired consistency. The mixture was trowel-mixed for another 4 minutes to ensure uniformity in the cement mortar. The resulting slurry was then transferred into a three-pong mold, measuring 40×40×160 mm for compressive strength tests and 100×100×100 mm for durability studies.

The molds were clamped onto a vibrating machine for 2 minutes to compact the mortar. Upon removal from vibration, the mortar prisms were immediately identified by their casting date and the type of cement used, denoted as 5-1-4, 5-4-1, 3-1-6, and 3-6-1, representing the mix mass ratio of OPC:CSA: CBW as detailed in Table 1.

To safeguard against moisture loss caused by evaporation, a polythene sheet that was impermeable and flat was used to cover the prisms. These prisms were then placed in a temperature-controlled room with relative humidity exceeding 90% for 24 hours±30 minutes, after which they were demolded and air-cured for 28 days. Similarly, PC specimens were also prepared for reference purposes, but potable water was used as the mixing liquid, and they were cured in water for 28 days.

2.2. Compressive Strength Testing

The 28-day compressive strength was determined using an automatic compression testing machine (model YAW-300) housed at Mombasa Cement Limited, a prominent cement manufacturing company in Kilifi County, Kenya. The testing procedure strictly followed the protocol outlined in KS EAS 148: 1 (2000).

2.3. Differential Thermogravimetric Analysis (DTA)

A Stanton Redcroft STA-781 device was used for the thermal analysis of raw clay, coconut shell powder, and hydrated cement. 25 g each of the clay, coconut shell powder, and hardened cement were placed in a platinum crucible and the thermal analyzer. The measurements were between

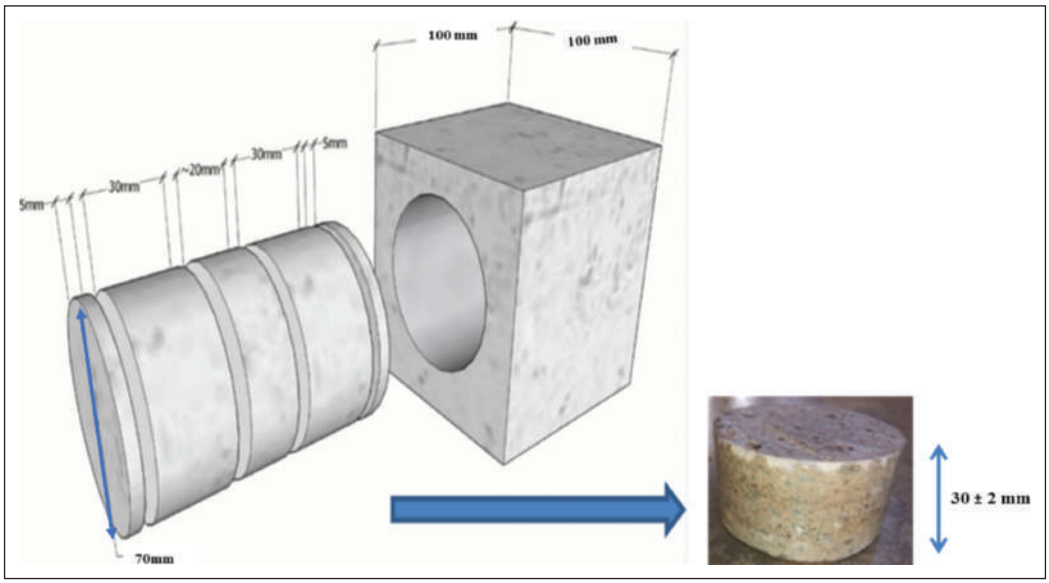


Figure 1. Preparation of specimens from the cube [16].

25 °C and 1000 °C, and the heating rate was set to 10 °C per minute. Thermal analysis of clay and powder samples was performed under atmospheric air conditions, whereas measurements for hydrated cement samples were conducted under a nitrogen atmosphere.

2.4. Durability Test

The experimental materials' permeability, sorptivity, Porosity, and durability were assessed by following the durability testing manual recommended by [16]. Two methods are available to evaluate the level of connectivity of pores in a concrete matrix: oxygen permeability index (OPI) and sorptivity [17]. The durability properties' quantification involves measuring the flow rate derived from Darcy's formula for laminar flow through a porous medium.

2.4.1. Preparation of Specimens for Durability Test

Durability tests were conducted following the protocol outlined by Alexander and coworkers [16]. Cement blocks of dimensions 100 millimeters that were allowed to harden for 28 days were bored perpendicular to the pouring direction and divided into slices, as illustrated in Figure 1, to obtain two specimens, each with a diameter of 70±2 millimeters and a depth of 30±2 millimeters.

The samples were labeled with an identifying number on their exterior using a permanent ink marker. Before experimentation, the labeled samples were permitted to dehydrate for seven days in a drying chamber regulated to 50 °C. After the samples were extracted from the drying chamber, they were cooled in an airtight container for 120 minutes until achieving a regulated indoor temperature of ±23 °C.

2.4.2. Oxygen Permeability Index Test

The South African standard [18], which prescribes the use of the oxygen permeability index (OPI), was used to assess oxygen permeability. The test setup consisted of a 70 mm diameter core fixed in a rubber sleeve and attached to a permeability cell, with a 30 mm thick piece as a cover concrete. The aim was to observe the oxygen pressure drop in this section. The method involved measuring the pressure decay of oxygen passed through a 30 mm thick slice (representing the cover concrete) of a 70 mm diameter core placed in a rubber collar secured on top of a permeability cell. Then, the permeability cells were placed in the test apparatus.

The cell was prepared for insulation by exposing it to an oxygen pressure of 100±5 kPa. The pressure and time factors were then recorded accordingly. The test was terminated 6 hours ±15 minutes after the start, or at a pressure of approximately 50 kPa, with pressure lags recorded at intervals of approximately 5 kPa. Using Equation 1, we calculated the Darcy permeability coefficient, K, in meters per second.

$$K = \frac{\omega V g}{RA}\frac{[d]}{[\theta.t]}\ln\frac{[Po]}{[P]} \quad (1)$$

Where K is the permeability coefficient in m/s; ω is the molecular mass of oxygen, 32 g/mol; V is the volume of oxygen under pressure in permeameter (m^3), g is the gravitational acceleration whose value is 9.81 m/s^2, R is the universal gas constant, 8.313 Nm/Kmol. A is the superficial cross-sectional area of the sample (m^3), d is the average sample thickness (m), **θ** is the absolute temperature (K), t is time (s) for pressure to decrease from Po to P, Po is the pressure at the beginning of the test (kPa), and P is the pressure at the end of the test.

Subsequently, the oxygen permeability index (OPI) was determined as in Equation 2.

Oxygen permeability index=-log (k) (2)

2.5.3. Testing for Sorptivity and Porosity

The disc samples were subjected to permeability and water sorptivity tests according to the protocols described in the durability handbook [16]. Samples were tapped up to 5 mm above the test surface to ensure the unidirectional flow of the caliper. They were then placed in a dish of calcium hydroxide solution, ensuring that the solution level was just above the edge of the sample. The samples were weighed at 3, 5, 7, 9, 12, 16, 20 and 25 minutes, respectively.

This was followed by vacuum saturation of specimens by applying 75 kPa suction. Finally, the specimens were submerged in water saturated with $Ca(OH)_2$ for 18 hours and fifteen minutes. The samples were re-weighed, and their Porosity was calculated using Equation 3.

$$n = \frac{M_{SV} - M_{SO}}{A.d.p_w} \quad (3)$$

Where: M_{sv} is the vacuum saturated mass of the samples to the nearest 0.01; M_{so} is the initial mass of the specimen to the nearest 0.01 g at a time to; A is the cross-sectional area of the specimens to the nearest 0.02 m^2; d is the average specimens' thickness to the nearest 0.02 mm; Pw is the density of water, 10^{-3} g/mm^3.

The mass of the water absorbed at each weighing period is calculated using Equation 4:

$$M_{wt} = M_{st} - M_{so} \quad (4)$$

Where: M_{st} is the mass to the nearest 0.01 g of the specimen at time t. Sorptivity was calculated from the slope of the graph of water absorbed (M_{wt}) versus the square root of time (an hour) using Equation 5.

$$S = \frac{F.d}{M_{SW} - M_{SO}} \quad (5)$$

Where: F is the slope of the best-of-fit line obtained by plotting M_{wt} against t½; S is sorptivity

2.5. Correlation Analysis for Permeability Test Parameters

The intercorrelations between the results of the permeability tests were compared with the compressive strength performances for all cement mixes produced. The factors correlating permeability included oxygen permeability index (OPI), Porosity, and sorptivity. Principal component analysis (PCA) was used to determine the correlation. A scree plot for the eigenvalues was plotted to determine the number of significant components. The "elbow" for the eigenvalues (Fig. 2) falls on eigenvalue 2, indicating two principal components. The first two factors explain a variance of 94.82%. The selected principal components were used to plot the loading, biplots, and score plots and analyze the existing correlations. Chemometrics Agile Tool (CAT) was used to perform the PCA, which works with the programming language R and the algorithm NAPLES (Nonlinear Algorithm for Partial Least Squares).

2.6. Migration Test

Following the procedures described in ASTM C1202-97 (2001), three samples of the 50% OPC replacement and the reference cement were allowed to cure in water for 28 days before being tested for accelerated chloride ion migration.

In an electrochemical test setup, 500 cm^3 of a 3.5% NaCl solution was added to the cathode compartment, while an equal volume of a 0.3 M NaOH solution was added to the anode compartment. Epoxy-coated mortar prisms were positioned in the test cell for each cement category. Stainless steel electrodes were attached, and the arrangement

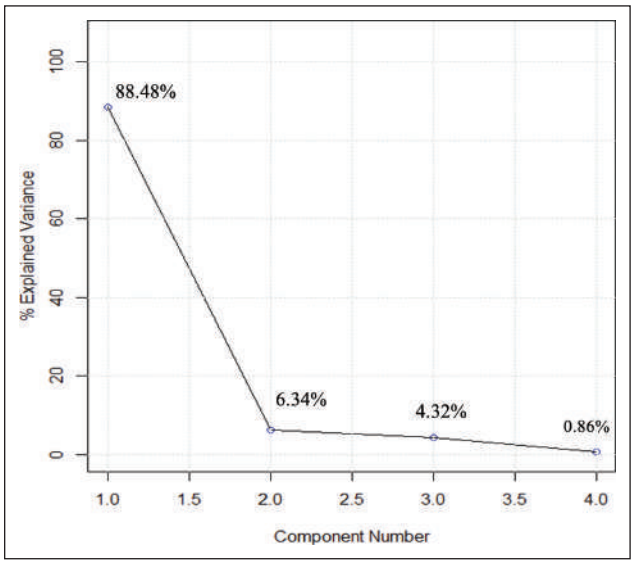


Figure 2. Scree plot for the eigenvalues.

was clamped in place. A potential difference of 12±0.1 V was applied for 36 hours, and the current was monitored every 30 minutes. The containers were covered with polyethylene paper to prevent evaporation, and glass rods were used to shake the solutions continuously. After exposure, the prisms were removed, the surfaces abraded, and cut into layers. Depending on the distance from the aggressive media, the samples were dried, pulverized, and packaged before being subjected to chloride analysis.

2.6.1. Chloride Analysis

10 g of ground samples were mixed with 75 ml of deionized water for one hour using a shaker. After a settling time of 30 minutes, the sample was treated with 25 ml of strong nitric acid to dissolve the cement lumps. The mixture was stirred, rinsed into a beaker, and allowed to stand for 4 minutes. The filtrate was heated and filtered. It was then poured into a volumetric flask. A sodium hydrogen carbonate solution was introduced, and water was added until the total volume reached 100 ml. The resulting solution was split into three equal parts, each titrated with a 0.1 M silver nitrate solution. This titration was performed three times on each part.

A chloride-free $CaCO_3$ blank was run through the same procedure. Using Equation 6, the concentration of chloride ions in the original sample was determined based on the titration results.

$$[Cl^-] = \frac{(V1 - V2)\ X\ 35.46\ X\ M}{V} \quad (6)$$

Where V_1 is the final volume of the extract, V_2 is the volume of the blank, V is the volume of silver nitrate, and M is the molarity of silver nitrate used.

2.6.2. Determination of Diffusion Coefficients

The standard procedures outlined in Kenyan standards [19] were adopted to determine the chloride concentration in the tested samples. These results were represented in chloride profiles. From the graphs, chloride diffusion

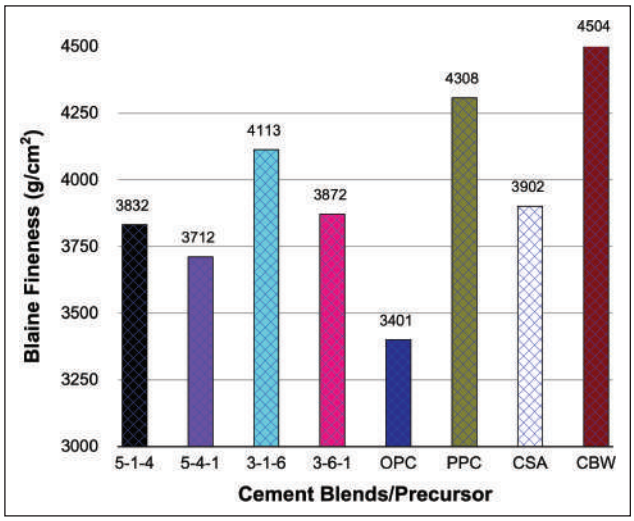


Figure 3. Binders mix blain fineness results.

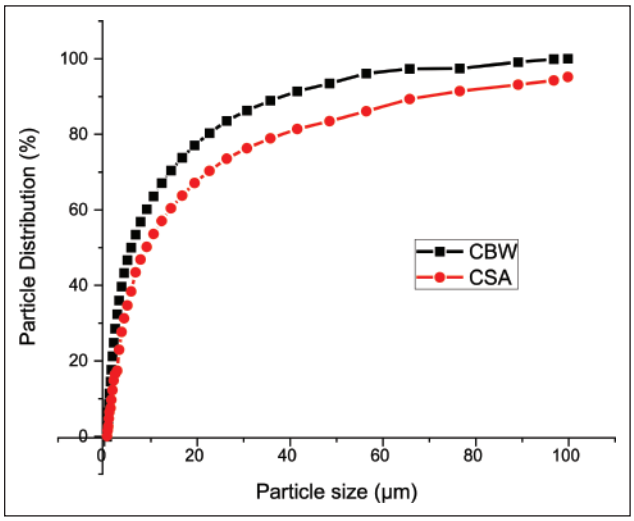


Figure 4. Particle size distribution results for CBW and CSA.

coefficients, D_{mig}, were derived from error fitting curves in Equation (7) using the method of least squares [20, 21].

$$\frac{\delta C}{\delta t} = D\frac{\delta^2 C}{\delta x^2} \quad (7)$$

C is the concentration of the Cl^- ions at a depth x, and at the moment, t and D are the diffusion coefficients.

The diffusion of chloride ions in concrete is approximated from the solution to Fick's second law equation [22] under non-steady-state conditions assuming boundary conditions boundaries $C_{(x,\,t)}$=0 at t=0, 0 < x < ∞ and $C_{(x,\,t)}$=Cs at X= 0, 0 < t <∞, constant ion interactions, linear chloride binding, and one-dimensional diffusion into a semi-infinite solid. Crank's solution to Fick's second law of diffusion is given by Equation 8.

$$C_{(x,\,t)}=C_{(s)}\left[1-\text{erf}\left(\frac{x}{(2\sqrt{D_{mig}\,t})}\right)\right] \quad (8)$$

The surface concentration ($C_{(S)}$), migration diffusion coefficient (D_{mig}), and the chloride ion concentration ($C_{(x,t)}$) at any depth (x) within the mortar bulk at time t constitute the equation. The Gaussian error function is obtained in computer spreadsheets as the error correction function, abbreviated as erf. Apparent diffusion coefficients, D_{app}, are calculated from the following equation [20, 21].

$$D_{app}=\frac{RT}{Z_i F}D_{mig}\frac{\ln t^2}{\Delta E} \quad (9)$$

In this context, R stands for the gas constant, F represents the Faraday constant, T indicates the electrolyte temperature measured in Kelvin, Zi denotes the valency of the ion ΔE refers to the effective applied voltage measured in volts, and t represents the duration of the test or exposure measured in seconds.

2.7. Determination of Thermal Resistance

The prepared mortar prisms (40 mm x 40 mm x 160 mm) of 5-1-4 and OPC cement paste were cured for 28 days and pressure tested after exposure to an electric furnace at 5.0 °C per minute. To maintain thermal stability for 60 minutes at the desired temperature, two thermocouples were used to measure the surface and internal temperature differentials. After allowing the samples to cool, they were weighed, and the thermal expansion was measured with a vernier caliper. Mass loss due to the high temperatures was measured with an electronic scale. The residual compressive strength was documented, and the thermal resistivity was calculated using Equations 10 and 11, considering both weight loss and strength loss as a measure of thermal stress.

$$W_L = \frac{W_1 - W_2}{W_1}\,X\,100 \quad (10)$$

W_1 and W_2 are the specimen weights before and after heating, respectively, and W_L is the loss in weight.

$$C_L = \frac{C_1 - C_2}{C_1}X100 \quad (11)$$

C_L is the loss of strength, while C_1 and C_2 are the compressive strength of the mortar before and after heating, respectively.

3. RESULTS AND DISCUSSION

3.1. Blaine Test of the Precursor Materials, Blended and Commercial Types of Cement

The specific surface area (SSA) is an essential factor in determining the reactivity of binders. Figure 3 represents the SSA for the binders. In this figure, the particles' specific surface area (in g/cm²) of the test materials is displayed as measured by the Blaine air permeability analysis

All the blended cement had higher SSA values above the minimum 3401 cm²/g of the standard OPC. The mechanically activated precursor (CSA/CBW) materials show high SSA of 3902 and 4504 cm²/g and are responsible for the overall high SSA in the binders.

Increased CBW substitution resulted in a higher surface area on the blended cement than the addition of CSA. As it reacts, a layer of hydration product forms around the outside of the particle, separating the unreacted core of the particle from the surrounding water. As this layer grows

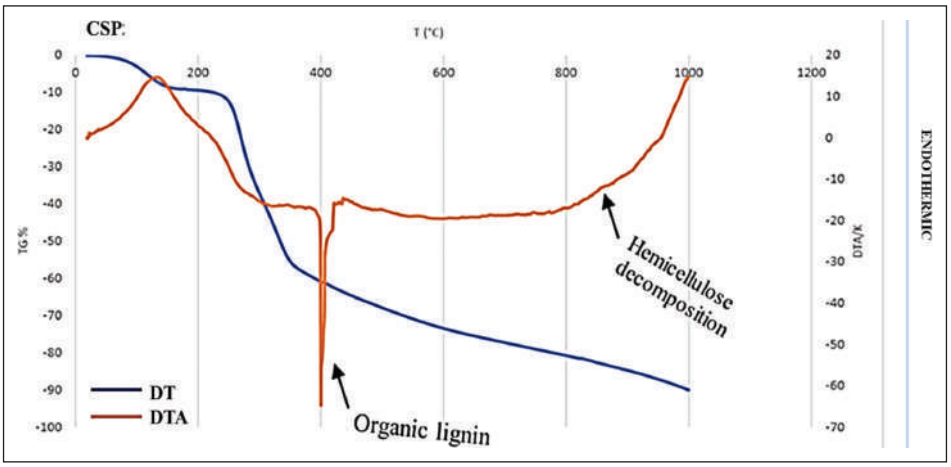


Figure 5. TG-DTA analysis for coconut shell powder.

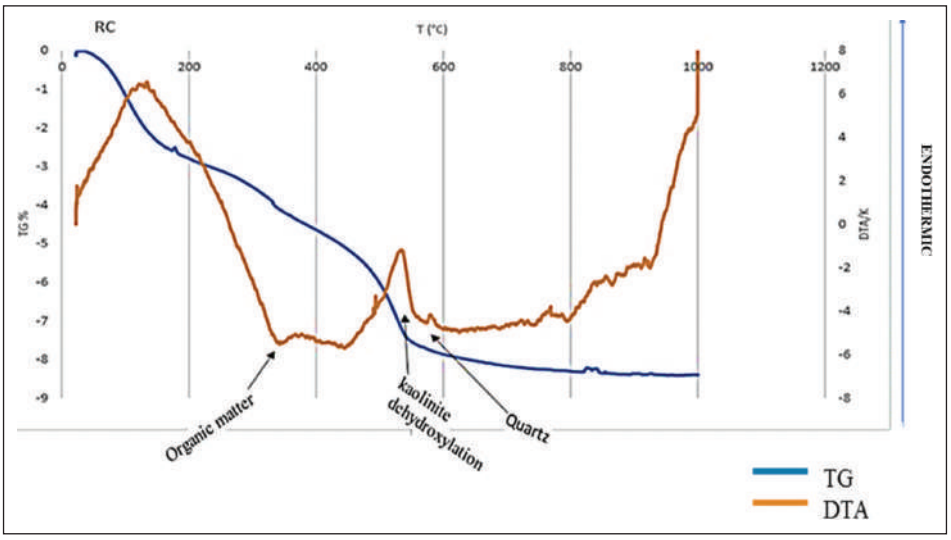


Figure 6. TG-DTA analysis for the raw clay sample.

thicker, the rate of hydration slows down [23]. This implies that a small particle will react faster than a large particle. Thus, CBW is mechanically more reactive than CSA.

3.2. Particle Size Distribution of the Precursor Materials

The particle size distribution of the mechanically activated CSA and CBW are represented in Figure 4. The particle size distribution of any cementitious material significantly affects its performance. The graph provides a detailed visual representation of the granular composition of these materials after mechanical activation. The particle size distribution of any cementitious material significantly affects its performance.

The CBW had a slightly higher particle size distribution compared to CSA, with more than 90% of its particles being below 45 microns in size, as shown in Figure 4. Thus, the CSA contains larger particles compared to CBW. This could result from the unburned carbon particles as heat in the furnace was not controlled. It is known that the material passing the sieve 45 μm is more reactive [24]. This indicates that both precursor materials are potentially mechanically reactive [25]. The reaction rate of the active precursor materials/cement particles primarily depends on their sizes. [26] worked on the microstructural and physical characterization of different solid wastes from clay bricks for reuse with cement. They observed that the clay brick waste sample particle with a small radius (large surface area) was more pozzolanic. Smaller particles hydrate more quickly in water than larger particles [27]. Typically, particles with a diameter of 1 μm react entirely in about one day, while one with a diameter of 10 μm reacts completely in about one month. It is assumed that one with a diameter larger than 50 μm never becomes fully reacted, even in the presence of a sufficient water source [27]. Arslan [28], in their study on the dissolution kinetics of iron oxide leaching from clays by oxalic acid, reported that small powdered particles [29] had a high dissolution.

3.3. Thermal analysis of the precursor

The thermal analysis carried out on the precursors used in this study is shown in Figures 5 and 6.

The graphs represent the various phase transformations that occur when coconut shell powder and raw clay are heated at different temperatures.

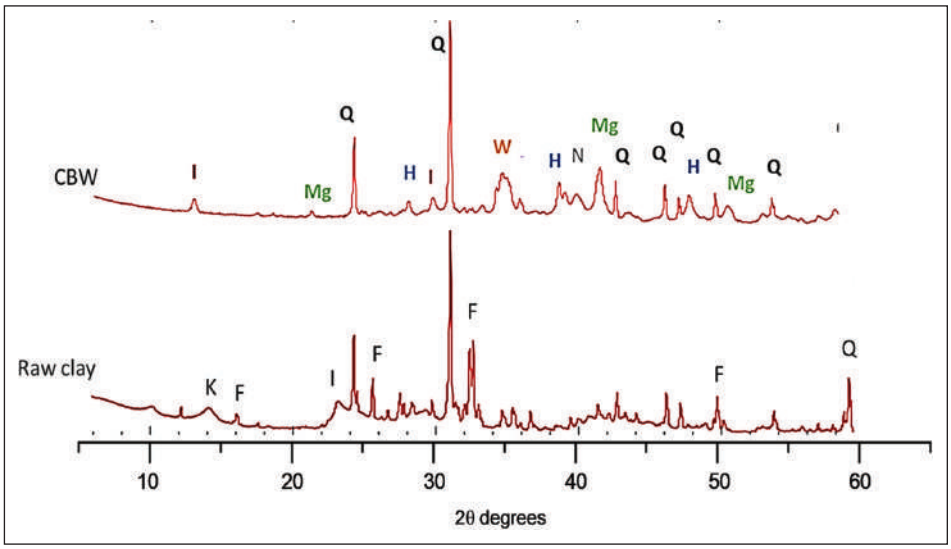


Figure 7. Comparison of the XRD pattern for the raw clay (top) and CBW (bottom) clay.

I: Illite; Mg: Magnetite; Q: Quartz; H: Hematite; W: Wollastonite; N: Nepheline; K: Kaolinite; F: Feldpar.

The TG/DTA analysis of the raw coconut shell powder shows a smaller region of mass loss at lower temperatures (below 250 °C), accompanied by an endothermic peak up to a temperature of about 150 °C. It could be associated with evaporation of the moisture [30]. This is preceded by a region of thermal decomposition and mass loss, followed by a sharp exothermic peak near 400 °C, further associated with the formation of coconut shell activated charcoal [31]. Additionally, it could be related to the combustion of the organic lignin/cellulose fraction. A broad endothermic peak with gradual mass loss is observed at temperatures above 800 °C. This was related to the thermal decomposition of hemicellulose. These findings agree well with previous work reported by [30], who obtained 38.44% and 47.54% mass loss between 200–280 °C and 280–365 °C, which was linked to the decomposition of cellulose and hemicellulose.

The TG-DTA graph of the clay sample is represented in Figure 6. An endothermic peak below 200°C is observed. This peak is associated with the thermal loss of physisorbed water within the clay interlayer, which is often mobile and loosely bound. At temperatures between 250 °C and 450 °C, an endothermic peak representing the dissolution of water molecules in the interlayer ions' initial strongly bonded coordination sphere is observed. This could further result from the hydroxylation of the functional groups connected to the clay minerals being removed at this temperature range [32]. According to Arslan [28], the condensation and dehydration of structural hydroxyl groups are indicated by an exothermic peak at 450–470 °C in the DTA curve.

An endothermic peak related to removing hydroxyl groups from kaolinite is observed at 550 °C. Similarly, at approximately 573 °C, a smaller peak is observed, indicating a transition from quartz-α to quartz-β [33]. The results also show a broad endothermic peak spanning from 600 °C to almost 940 °C, which is attributed to the dehydroxylation of the silica-alumina content present in illite, forming an amorphous substance. At temperatures above 950 °C, a sharp exothermic peak is detected, indicating the formation of crystalline silica-alumina phases. These findings suggest that the optimal temperature for calcination of kaolinite clays should be below this threshold [34].

3.4. Mineralogical Analysis of CBW and CSA

The mineralogical analysis of the precursor materials of the blend cements is shown in Figures 7 and 8. The figures show various minerals present in raw and calcined clays.

The XRD pattern for the raw and CBW clay (Fig. 7) reveals the presence of various minerals, including illite, magnetite, quartz, hematite, wollastonite, nepheline, kaolinite, and feldspars. The calcined clay brick waste shows the disappearance of the kaolinite upon thermal treatment, whereas illite loss of crystallinity is evident. Furthermore, a collapse of the illite interlayer is observed, with the basal peak shifting to a higher 2θ value. Additionally, hematite and magnetite (Fe oxides) formation is noted, along with the disappearance of feldspars and the emergence of wollastonite and nepheline.

The results in Figure 8 show an XRD analysis of the CSA, revealing a series of peaks associated with crystalline SiO_2 (quartz). These features may indicate burning temperatures exceeding 700 °C [35]. Peaks related to K-chlorate, a phase previously observed in vegetable ashes burned at temperatures above 400 °C, are also identified [36]. The two broad scattering haloes observed around 20° and 27° 2θ angles are related to an unburned organic fraction [37].

Figures 7 and 8 show silica-alumina minerals' presence in the two precursors. Calcined clay, with its high alumina and silica content, promotes the formation of calcium-silicate-hydrate (C-S-H) and calcium-aluminate-silicate-hydrate (C-A-S-H) gels, enhancing the mechanical properties and durability of HACs. The mineralogical compositions of pozzolanic precursor materials, such as CBW and CSA, play a pivotal role in the hydration process and microstructure development in hybrid alkaline cement [38]. Rich in silica, the ash from coconut shells aids in the creation of C-S-H and refines the pore structure, creating a matrix that

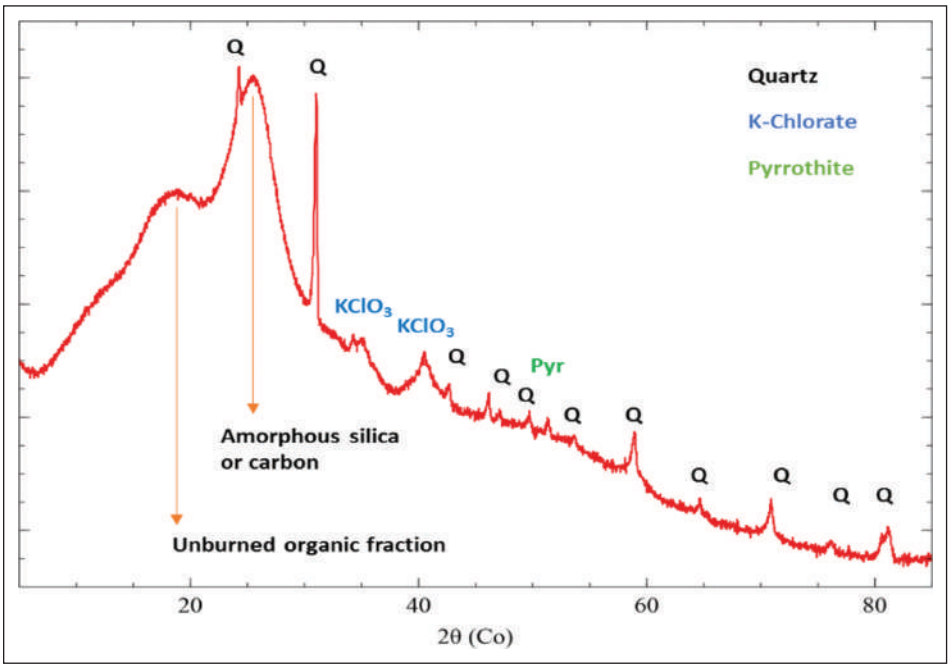


Figure 8. XRD pattern of coconut shell ash (CSA).

is more robust and compact [39]. Recent studies further highlight the importance of understanding the mineralogical properties of these precursors to optimize the performance of hybrid alkaline cement [40, 41].

3.5. Compressive Strength Test for Cement Mortars

The compressive strengths development of the binders (3-6-1, 3-1-6, 5-4-1, and 5-1-4) activated by different concentrations of Na_2SO_4-alkaline activators (0.0, 0.5, and 2 M) and different OPC:CSA:CBW ratio at 28 days of curing are shown in Figure 9. They are compared to conventional cement.

Generally, all blended cement prepared using water exhibited low compressive strength compared to alkali-activated blends and OPC (Fig. 9) after 28 days. This could be attributed to the slow strength development due to the incorporated pozzolana's slow reaction nature. The OPC substitution effect is demonstrated by decreased compressive strength across all the blends with OPC substitution from 50% to 70%. The strength of OPC was almost double that of 70% replacement, with 3-6-1 giving the lowest strength. This can be explained by more proportionate unreacted filler materials (CSA/CBW), hence weak bonding among them [42].

The results show that each formulation (50 and 70 OPC replacement) with high CBW replacement exhibited high compressive strength. Fine particles of calcined clay can explain this and are bound to fill the pores more effectively, resulting in a denser and stronger matrix. Grinding calcined clay brick waste reduced accumulation and decreased the average particle diameter, improving its reactivity and performance in the cement matrix. The optimal particle size distribution ensures better packing density and enhances the mechanical properties of the cement, particularly its compressive strength [43].

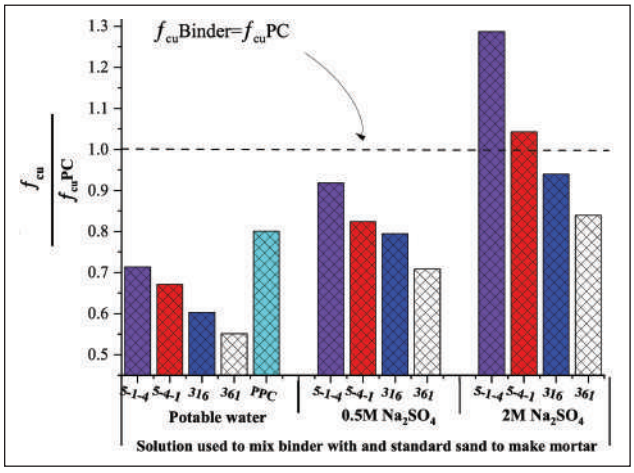


Figure 9. 28-day compressive strength (fcu) results for 0.5 w/c binder mortars compared to Portland cement.

The compressive strength of the activated blended cement achieved about 30% and 50% increase with the addition of the 0.5 M and 2 M Na_2SO_4 in each blend. A considerably significant increase in compressive strength with alkali activation addition in H_2O<0.5 M<2 M across all blends is observed. The 50% OPC replacement blends displayed better compressive strength performance than OPC at 2 M Na_2SO_4, with 5-1-4 having the highest compressive strength. The presence of SO_4^{2-} ions in the activator solutions within the cement mortar matrix may explain why chemically activated mortars achieve greater compressive strength values. The amount of alkaline activation products (gels) formed is responsible for the mechanical development of the alkaline hybrid binders [44].

3.6. Durability Index (DI) Test Results

Based on the details provided by Bakera and Alexander [45], this is a synopsis of the findings of the DI tests for oxygen permeability and water sorptivity using CBW and

Table 2. Judgement criteria for the quality of concrete durability index (DI) tests

Qualitative description	Oxygen Permeability Index (OPI) log scale	Water Sorptivity Index (WSI) mm/h$^{0.5}$
Excellent	>10	<6
Good	9.5–10	6–10
Poor	9.0–9.5	10–15
Very poor	<9	>15

CSA. The quality of the concrete was evaluated using the standards laid out in Table 2.

Sorptivity measures the rate of fluid movement through the concrete under capillary suction, while OPI measures the degree of interconnectivity of the pores in the matrix. The Porosity of the cement mortar and the sorptivity are influenced by the degree of hydration and the ratio of weight to cement [46]. The permeability of the sample decreases with increasing OPI value and vice versa. Conversely, high sorptivity/porosity values of cement matrix indicate high permeability. Permeability determines how easily liquids can penetrate and flow through the concrete when exposed to a pressure gradient.

3.6.1. Binder Oxygen Permeability Index

The oxygen permeability test results for different binder types cured for 28 days are given in Figure 10. The figure illustrates the variation in permeability based on precursor content and alkali concentration. The values provide a quantitative measure of the concrete's resistance to oxygen ingress, with higher OPI indicating lower permeability and enhanced durability.

The results, based on Durability Index (DI) judgment criteria in Table 2, show that all blended cement mortars prepared using water had OPI values below 9.5 (log scale), signifying "poor" quality. This value was lower compared to PPC and OPC mortar. As can be observed in Figure 10, there was a notable decrease in OPI in blended cement in the order 5-1-4>5-4-1>3-1-6>3-6-1. This order was replicated for the blends prepared with the activator at the two different concentrations. Hybrid alkali-activated mortars exhibited higher OPI compared to the respective non-activated mortars. They had values above 9.5 (log scale), which signifies "good" quality. There was also an increasing trend in OPI values with an increase in the concentration of Na_2SO_4, the alkali activator, for each cement mix. The 2 M Na_2SO_4 HAC showed higher OPI values than those of 0.5 M Na_2SO_4, with all having OPI values above 10 (log scale), which signifies "excellent" quality. This could be attributed to the presence of SO_4^{2-} ions in the activator solutions in the cement mortar matrix. SO_4^{2-} in mortars has been reported to form ettringite crystals, which fill the hardened cement mortar cracks and pores, lowering the permeability [47]. The ettringite formation is as shown in Equation 12.

$$6Ca^{2+}+2[Al(OH)_4]^-+3SO_4^{2-}+26H_2O \rightarrow Ca_6Al_2(SO_4)_3(OH)_{12}.26H_2O \quad (12)$$

The formation of this product in the early days of curing causes densification of the hardened cement matrix.

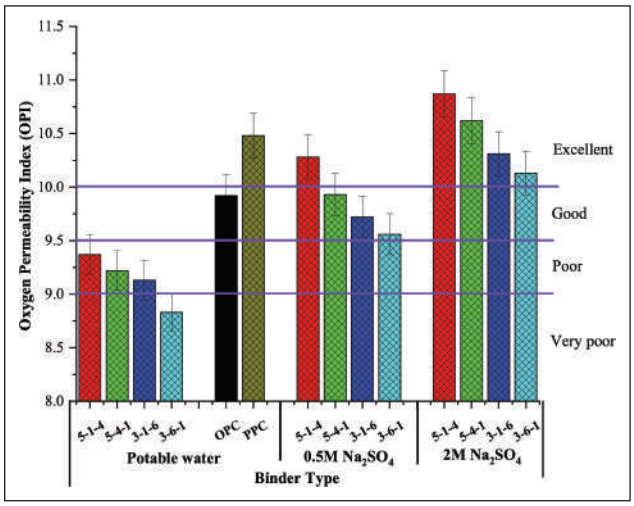


Figure 10. Oxygen permeability index (OPI) results for 0.5 w/c binder mortars cured for 28 days.

It was clear that the substitution effect was a significant factor in the development of the cement matrix. A negative OPI response was pronounced on the increased substitution of CSA compared to that of CBW. This could be linked to the powder's particle size distribution, which is not uniform. The pozzolana "micro-filler effect," in the fine and ultrafine size range in combination with Portland cement, can also enable higher packing densities of the mortar or cement mixture [48]. Heterogeneous nucleation can also be attributed to this effect as a second physical phenomenon that could be significantly related to small particle size distribution. The pozzolana fine particles settle between the clinker crystals, lowering the energy barrier to allow hydrates to form on foreign fine particles. The finer the particles, the faster the reaction. This aspect could contribute positively to the quality of permeability property of 5-1-4 compared to 5-4-1 and 3-1-6 compared to 3-6-1 mortar cement.

Generally, all the HAC blends offered reduced permeability. This could be linked to refined pore structure and the ability to bind chloride ions chemically, limiting chloride ingress and protecting the concrete. Additionally, their high alkalinity maintains a protective passive layer on the steel. These properties make hybrid alkaline cements particularly durable in chloride-rich environments like marine settings and roads treated with de-icing salts [49]. After 28 days of curing, hybrid alkaline cement blends exhibit superior resistance to chloride ion penetration compared to traditional Portland cement, highlighting their enhanced durability in aggressive environments [50]. Continuous curing after 28 days [51] reported significantly improved flexural strength, compressive strength, and resistance to chloride penetration of alkali-activated slag mortar with 2–3% alkali contents.

3.6.2. Porosity of Different Mortars Tested

The Porosity of the different mortars tested is given in Figure 11. The graph with a high porosity indicates a high chance of fluid penetration into the mortar matrix. This highlights the variation in Porosity across the samples,

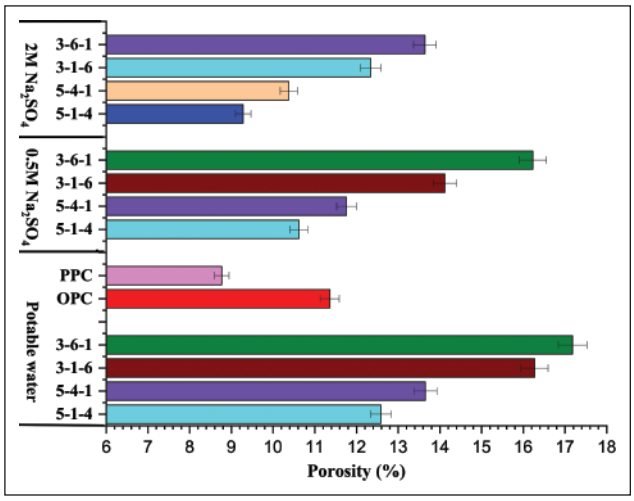


Figure 11. Porosity (%) results for 0.5 w/c binder mortars cured for 28 days.

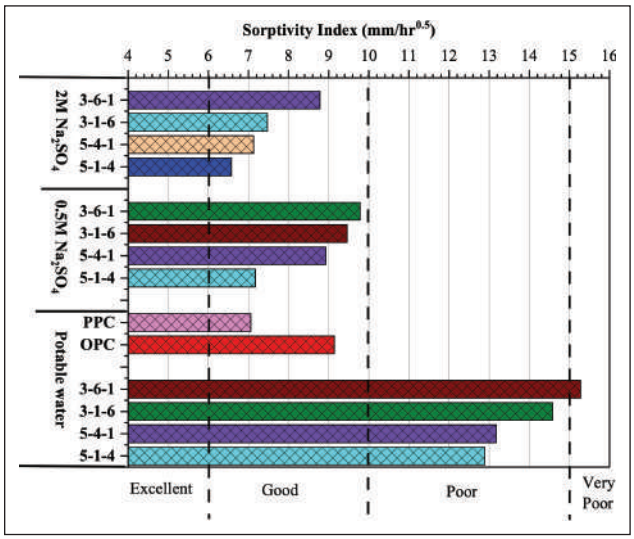


Figure 12. Sorptivity results for 0.5 w/c binder mortars cured for 28 days.

which directly impacts their mechanical and structural properties and, thus, their performance under different aggressive environments.

All the blended binders in water exhibited higher Porosity compared with OPC mortars (Fig. 11). This trend is more pronounced at a higher precursor replacement of 70%. The blend containing 60% CSA displayed the highest Porosity of 51% higher than the standard OPC mortar. Based on these findings, it appears that the pore structure of the OPC mortar is more complex and intricate than that of mortars made with pozzolana cement. The presence of more visibly enlarged macropores in the pozzolana mortar during its early curing stages could be the reason behind this [52]. The reaction of pozzolanic precursor materials with $Ca(OH)_2$ is a slow process, forming calcium-silica-alumina (C-S-A) gel, an insoluble cementitious material [47]. The formed insoluble crystalline particles may fill the pores of the hardening concrete, making it dense with refined pores at a later age.

Compared to non-activated mortars, alkali-activated hybrid mortars reduced Porosity by more than 10% in all cement categories. The 5-1-4 hybrid mixture of 0.5 M and 2 M Na_2SO_4 showed the highest reduction in Porosity at 19% and 36%, respectively, while the 3-6-1 mixture showed the lowest reduction at 6% and 26%, respectively. Increasing the dosage of Na_2SO_4, an alkali activator, also showed a similar trend. The corresponding 2 M Na_2SO_4 HAC showed lower Porosity than 0.5 M Na_2SO_4 HAC. This could be due to the low water absorption in the OPC hybrid copolymer due to the presence of chemical activators that increase the dissolution and gel formation of silica and alumina, resulting in the formation of more C-S-H gels and AFm-type phases as well as C–A–S–H with longer chains. The dense C-S-H gels formed by the chemical activation of aluminosilicate materials such as calcined clay brick waste/coconut shell ash lead to reduced Porosity in the properties of the chemically activated materials [51]. The C-S-H gels formed during the dissolution and gelation of silica and alumina are structurally similar to those formed during the hydration of cement [53].

According to Angulo-Ramírez et al. [54], the low Porosity of HB mortar indicates that the pores have been refined and the pore network in this system has become more tortuous. Compared to OPC, hybrid cement mixtures exhibit exceptional pore refinement [55]. This behavior can be associated with the potential of the blended cement structure to reduce Porosity and compactness, which were caused by the existence and production of a strongly cross-linked gel (C-A-S-H) with longer chains than the C-S-H gel commonly seen in Portland cement. The good behavior of alkali-activated CBW- CSA mortar is generally explained by the coexistence of aluminosilicate gels, such as C-A-S-H.

3.6.3. Water Sorptivity Test of Different Mortars Tested

The water sorptivity test results for various binder types, all cured for 28 days, are given in Figure 12. The different binders include OPC, PPC, and CSA/CBW blended cement prepared in water and activated with alkali. This highlights differences in water absorption rates, directly influencing the material's durability and long-term performance. The results provide the suitability of each binder type for use in environments where moisture exposure is a concern.

Hybrid cement prepared with 2 M Na_2SO_4 had lower sorption capacity than those prepared with 0.5 M Na_2SO_4, suggesting that the Porosity of the chemically activated cement decreases with increasing Na_2SO_4 concentration. In alkali-activated cement, chemical activators promote the dissolution of silica and alumina, which favors C-A-S-H gel formation; this could be the reason for the low water absorption of the cement. Since aluminosilicate materials such as CBW-CSA form dense C-A-S-H gels, chemically activated cement has a lower sorption capacity [56]. The architectures of the C-A-S-H gels are similar when the cement is hydrated or activated with alkali [53]. An alkali activator ranging from 0 M to 4 M NaOH was used by [57] to activate phosphogypsum binders and ground granulated blast furnace slag. Their data showed that low molarity was the most porosity-promoting factor.

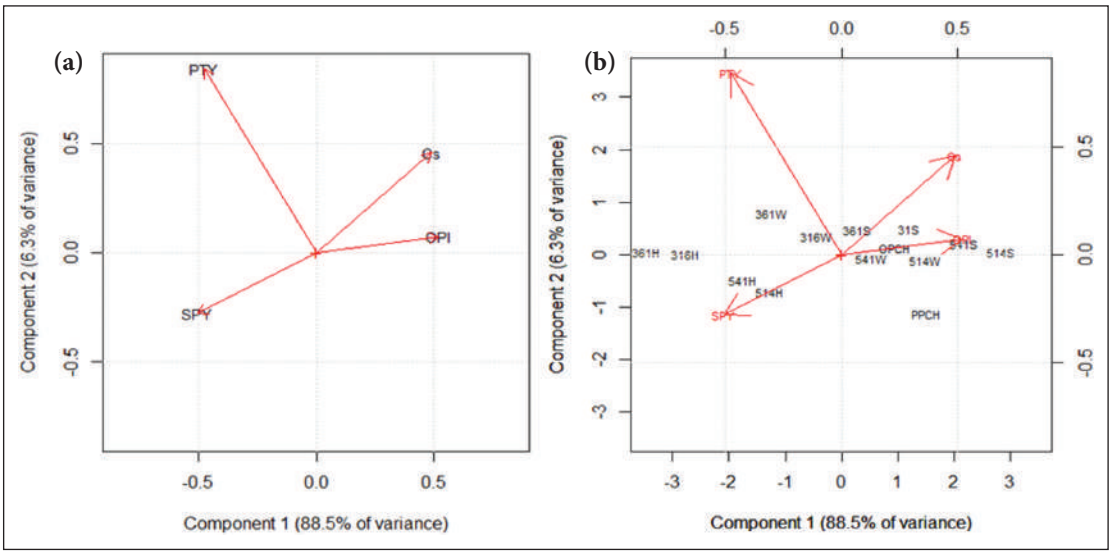


Figure 13. 2D factors loading plots and biplots. **(a)** Loading plot (94.8% of total variance). **(b)**Biplot (94.8% of total variance).

OPI: Oxygen Permeability Index; Cs: Compressive strength; PTY: Porosity; SPY: Sorptivity; 361H, 316H, 541H, and 514H are blends prepared with water, 361W, 316W, 541W, and 514W are blends with 0.5M Na_2SO_4 and 361S, 316S, 541S, and 514S are blended with 2M Na_2SO_4.

In this study, sorptivity reduced as the CBW/CSA ratio increased, according to experiments with varying ratios (1:4 to 4:1). Sample 5-1-4 showed decreased sorptivity independent of the alkali concentration. This could be associated with the high specific surface area of CBW (Fig. 3) in hybrid-blend cement that has been found to enhance its durability significantly. Nano-sized particles, such as nano-silica, improve cement's mechanical properties and durability by filling micro-pores and refining the pore structure. This optimization leads to a denser microstructure, which enhances resistance to water and chloride ingress, ultimately increasing the lifespan of the cement. Additionally, these nanoparticles promote secondary hydration reactions, further contributing to improved durability by creating additional C-S-H gels, which are crucial for the structural integrity of the cement [58]. The activation conditions and precursor characteristics significantly affect the hybrid binder's effectiveness, as stated by Balun and Karataş [59]. The results obtained by Bernal and colleagues [60] from their investigation into the engineering and durability properties of a combination of slag and alkali-activated metakaolin were similar. The results showed that water absorption and permeability were reduced when activator concentrations were increased and metakaolin was substituted within a specific range.

According to several researchers, chemically activated cements have shown mixed results in water absorption and permeability compared to OPC concretes. While using slag as the precursor, Mithun and Narasimhan [61] found that an alkali-activated binder had lower total Porosity, less water absorption, and less chloride ion penetration than an OPC. Air permeability and sorptivity are two areas where AACs made of slag typically underperform regular concrete for a given strength grade [62]. Similarly, Albitar et al. [63] noted that compared to geopolymer concrete, OPC concrete exhibited reduced sorptivity and water absorption. Precursors, activators, specimen maturity, and testing procedures are potential causes of the observed discrepancy between hybrid binders and OPC [64].

3.6.4. Correlation Analysis for the Permeability Test Results

The PCA projection of the factors in the 2D-factor loading space is shown in Figure 13a. The 2D loading plot for the factors is consistent with the previous observations in the literature.

The compressive strength (Cs) and the oxygen permeability (OPI) are projected in the same direction, signifying that they are strongly correlated. This implies that blends with high compressive strength have high OPI and vice versa. On the other hand, the Porosity and sorptivity are projected in the same direction, opposite to compressive strength and OPI, demonstrating the existing inverse relationship between these factors. The biplot, Figure 13, associates cement blends with 2 M Na_2SO_4 activator (361S, 316S, 541S, and 514S) and OPC with a significant correlation with compressive strength and OPI. It can be concluded that these blends performed better and attained higher OPI and compressive strength due to lower Porosity and sorptivity and, thus, lower permeability.

The blends prepared with water only are all projected to the left, correlating strongly with sorptivity and Porosity. It can be concluded that these blends had lower performance in terms of compressive strength and higher permeability. Meanwhile, the blends with 0.5 M Na_2SO_4 activator lie between the two distinct later observations. Thus, intermediate permeability performance.

The compressive strengths for the cement mixes projected in the 2D score plot Figure 14a–d are consistent with the predictions in the loading plots and biplots. Blends prepared with 2 M Na_2SO_4 activator (361S, 316S, 541S, and 514S) and

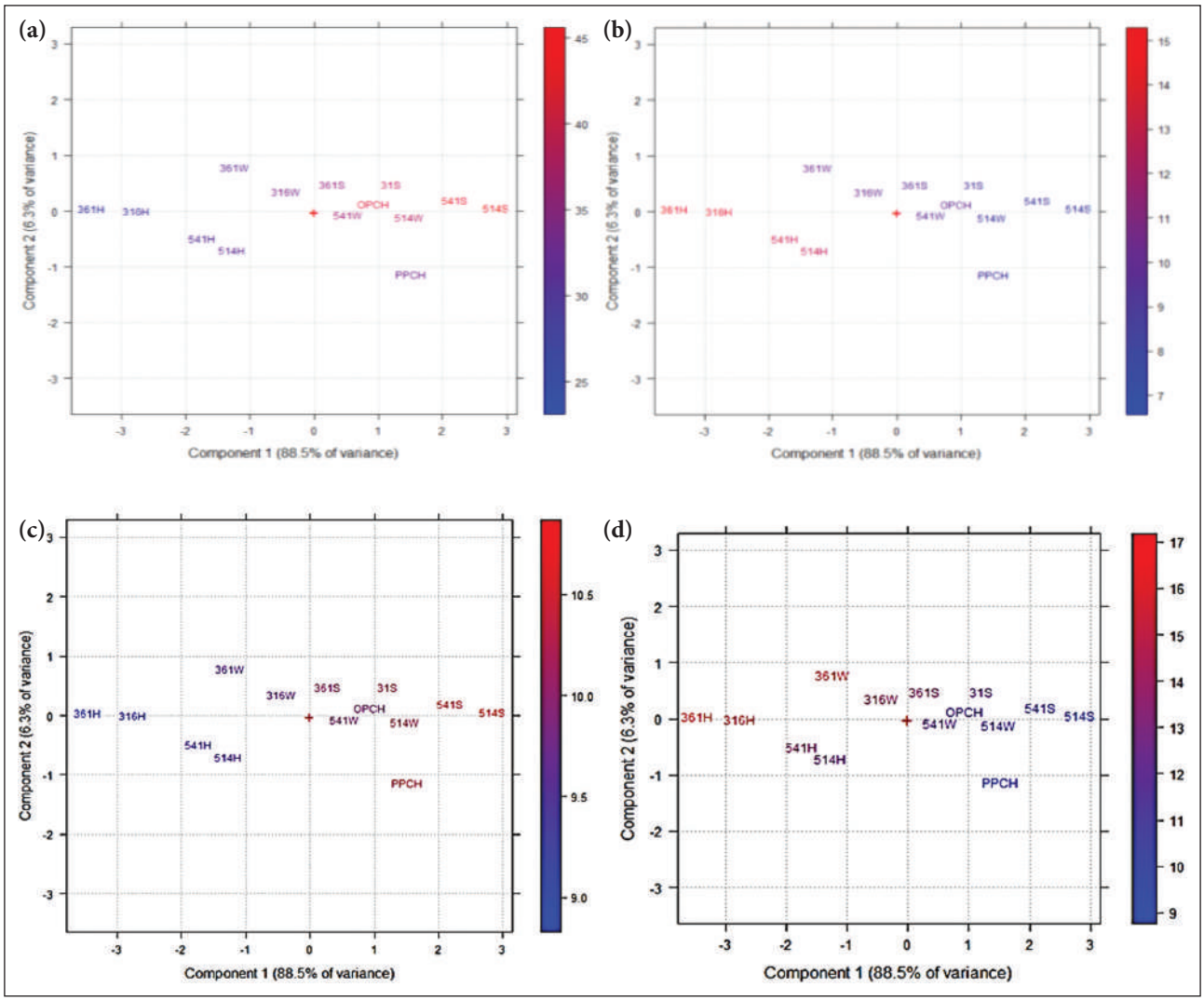


Figure 14. Color score plots for the projected factors. **(a)** Score plot (94.8% of total variance) color scale: Cs. **(b)** Score plot (94.8% of total variance) color scale: SPY. **(c)** Score plot (94.8% of total variance) color scale: OPI. **(d)** Score plot (94.8% of total variance) color scale: PTY.

361H, 316H, 541H, and 514H are blends prepared with water, 361W, 316W, 541W, and 514W are blended with 0.5M Na_2SO_4 and 361S, 316S, 541S, and 514S are blended with 2 M Na_2SO_4.

OPC demonstrate the highest compressive strength, OPI, and lowest Porosity and sorptivity. This is also the case with OPC. Blends prepared with water only are associated with the weakest strengths and OPI and higher Porosity. Blends with 0.5 M activator show average performance between -1 and +1 of component 1, which correlates with intermediate performance. The PCA, therefore, clearly categorizes the different blends into distinct performances about permeability, with 2 M Na_2SO_4 activator blends showing the best performance.

3.7. Chloride Ingress

3.7.1. Chloride Profiling

The chloride profiles against the depth of cover of each category of the mortar cubes are shown in Figure 15. These involved determining the concentration of the chloride ions ($\times 10^{-10}$ g/g) at different depths of the test binders' mortar bulk at 0.5 w/c ratios.

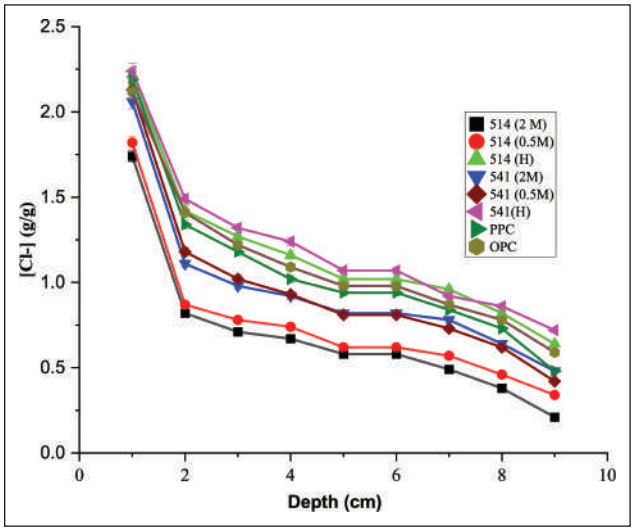


Figure 15. Chloride ions concentration at different depths of penetration for 0.5 w/c binder mortars cured for 28 days.

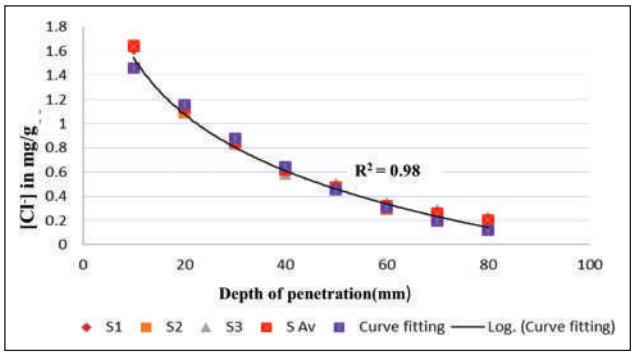


Figure 16. Chloride error function fitting for 5-1-4 (2 M).

D_{app}=4.20 x 10^{-10} m^2/s, and Cs=1.89% (R^2=0.98).

3.7.2. Apparent Diffusion Coefficients for Chloride Ions

Figure 16 displays the error fitting curve for calculating the apparent chloride diffusion coefficient (D_{app}) for the test binder, 514 (2 M) mortar. The chloride apparent diffusion coefficients for each binder category were found using similar error-fitting curves. Table 3 also shows the D_{app} statistics for each binder group.

As the penetration depth increased, the total chloride was observed to be reduced across all binder types (Fig. 15). The alkali-activated blends, blended with more calcined clay brick waste, compared to coconut shell ash, showed an increased reduction in chloride penetration. The chloride concentration in all binders drops drastically at a depth of less than 2 cm. The exposed surface's proximity to the aggressive medium may explain this. Every form of cement binds a certain amount of chloride. Chloride binding slows the chloride's diffusion into the binder's bulk. As observed by Ngui et al. [65] this can be explained by the cement mortar's chloride ion binding capability and diffusivity penetrating the cement mix.

According to the profiles, PPC had less chloride infiltration and a lower D_{app} than OPC (Fig. 15 and Table 3). Moderately substituted pozzolana cements have been found by other researchers to have a lower diffusion coefficient [66]. The pore solution of mixed cement contains less CH than that of OPC, which could explain this. According to Wang et al. [67] blended cement has a low CH content because of a pozzolanic reaction source, the source primary OH and -source; a reduction in OH-concentration reduces the pore water's ability to exchange OH for chlorides [68]. Blended cement is particularly effective in lowering chloride-induced corrosion due to higher aluminate contents than plain Portland cement. Al_2O_3 is known to bind Cl- ions, forming Friedel's salt. This enhances the chloride binding capacity, decreasing the free chlorides resulting in lower chloride ingress. Tang et al. [69] noted that the C-S-H gels, particularly in blended cement with a low calcium-to-silicon ratio, react with chloride salt, producing Friedel's salt. This salt can seal the interior pores, improve the distribution of pore sizes, and make the material more resistant to corrosion caused by chloride ions.

The results (Fig. 15 and Table 3) showed that increasing CBW from 1 to 4 decreased the D_{app} at all mixing liquids. The converse was true of D_{app} on increasing CSA. Thus, the blended cement's D_{app} was 5-1-4<5-4-1 at all mixing liquids.

Table 3. D_{app}, R^2, and Cs (%) values for different cement mortars

Binder type	D_{app} (x 10^{-10} m^2/s)	R^2- Value	Cs (%)
5-1-4 (2 M)	4.20	0.99	1.89
5-1-4 (0.5 M)	4.91	0.98	1.92
5-1-4 (H)	7.37	0.97	2.34
5-4-1 (2 M)	5.83	0.98	2.23
5-4-1 (0.5 M)	6.32	0.97	2.21
5-4-1 (H)	8.66	0.96	2.37
OPC	6.65	0.97	1.92
PPC	6.48	0.97	2.37

OPC: Ordinary portland cement; PPC: Pozzolanic portland cement.

This supports the argument in 3.3 of CBW's superior mineralogical properties compared to CSA Figures 7 and 8. This contributed positively to the mortar microstructural development [24, 70]. Alkali-activated blend cement offered greater resistance to chloride ingress than OPC at any given alkali concentration. There was an increasing trend of D_{app} with the increase of alkali-activator concentration as well as the increase of CSA from 1-4 as [5-4-1(H) < 5-1-4(H) < PPC] < OPC < [5-4-1(0.5 M) < 5-4-1(2 M) < 5-1-4 (0.5 M) <5-1-4 (2 M)]. The introduction of an alkali activator increases the rate of alumina-silicate dissolution. As a result, the concrete becomes denser, attains higher resistivity, and reduces chloride diffusivity due to the greater cementitious material produced by the more pozzolanic reaction. The cementitious material can be produced via alkali-activated cement with increased time [71]. According to Abdulkareem et al. [72], this causes the final mortar or concrete to have less permeability. Chemical activation at an 80% BFS replacement level with a high dose of 10.17 kg/m^3 KOH was able to speed up hydration and portlandite consumption, according to [72].

3.8. Thermal Resistance

After exposure to various thermal loads, quantitative evaluation of the hardened paste behavior was determined by measuring their residual strengths following heat exposure. Heat strength profiles of 5-1-4 and OPC pastes binders after being heated to 100, 300, 500, 700, and 800 °C are displayed in Figure 17.

On exposure of cement paste to temperatures ranging from 25 to 100 °C, OPC's compressive strength dropped sharply while 5-1-4 blends increased marginally (Fig. 4). According to Zivica et al. [73], crystalline products can be formed in the structural pores of pozzolana blend and alkali-activated paste when the reaction rate of the unreacted materials is increased by raising the temperature. A possible explanation for OPC's weakening at 0 to 100 °C could be pore water evaporation. At temperatures between 100 and 300 °C, the compressive strength of 5-1-4 blends rapidly decreased. The loss of water content in the specimens is likely to cause this. Free and chemically bonded water within specimens swiftly migrates to the surface and evaporates as the external temperature rises from ambient to 300 °C. This leads to a quick loss of strength in the 100–300 °C range and harms the specimens' internal microstructure [74]. Once the temperature reaches 300 °C, the strength of 5-1-4 blends gradually de-

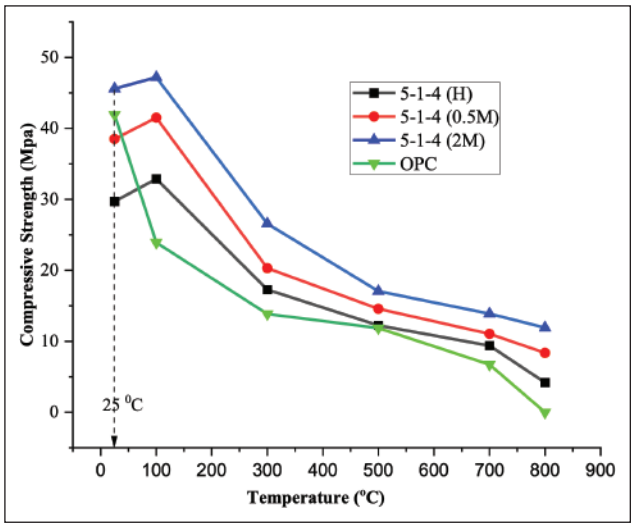


Figure 17. Results of the effect of heat on 5-1-4 blends compared to OPC.

creases in the order of 5-1-4 (2M) < 5-1-4 (0.5M) < 5-1-4(H), indicating a small impact of temperature on strength deterioration in that order. Deterioration in strength also slows down about 300 °C because water evaporation decreases.

OPC at temperatures beyond 300 °C continued to show a relatively steady decrease in compressive strength to total failure at 800 °C. This could be associated with the deterioration of the CSH and Ca(OH), the principal binding phases of the hydrated OPC mortar. OPC has previously indicated an irreversible loss of strength at a temperature above 200 °C [75]. Jeon et al. [76] reported that the main cause of OPC strength reduction on exposure to high temperature was mainly due to the expansion of lime after chilling and that the breakdown of $Ca(OH)_2$ had minimal impact. The OPC system was found to degrade at elevated temperatures up to 600 °C, while Rashad [77] found that Na_2SO_4-activated slag exhibited superior resistance. Their research showed that a higher concentration of Na_2SO_4 and finer slag resulted in superior heat resistance.

Figure 17 shows that at room temperature and after exposure to high temperatures, the compressive strength of CBW-CSA-blend pozzolana and alkali-activated-based paste is greater than that of OPC mortar. Because of this, structural components made with CBW-CSA blend alkali-activated-based mortar can offer the same or even greater fire resistance, and there are many other environmental benefits, including reduced energy consumption and carbon dioxide emissions.

4. CONCLUSION

The described study examined the effects of thermal stability and aggressive media on a cement blend of activated clay brick waste and coconut shell ash. The current findings demonstrate that CSA and CBW, when added to alkali-activated cement mortar, considerably enhance its prospective durability about thermal resistance, compressive strength development, and penetrability (sorptivity, permeability, conductivity, and diffusion). The results show that blend alkali-activated cement mortar can be made of higher quality using CSA and CBW. In most cases, a 5:1:4 ratio of OPC to CSA to CBW and a concentration of alkali activator up to 2 M Na_2SO_4 yield better results. This is because CSA and CBW can change the chemical and physical microstructure of the mortar that has been activated with alkali. It is important to take note of the following findings from the tests.

1. All blended cement had high Blaine values compared to the standard. The Blaine values, which were directly proportional to the particle size distribution of the precursor materials, gave high reactivity, which is seen to be contributed by an increase in CBW content. The formulation of 5-1-4 with a high composition of CBW gave an improved compressive strength at all concentrations compared to the corresponding samples of 5-4-1. In potable water, the compressive strength 5-1-4 was almost double that of 5-4-1.
2. When the concentration of the alkali activator was increased by using 0.5 M and 2M, the outstanding 5-1-4 HAC blend exhibited a compressive strength growth of 30% and 50% concerning the water-prepared blends. Compared to non-activated mortars, alkali-activated blend mortars showed more than 10 percent decreased sorptivity, Porosity, and OPI across all cement categories.
3. Regarding the DI test results, CBW properly mixed with CSA generally produced an excellent binder, which improved with a higher content of CBW than CSA and at a higher alkali concentration. 5-1-4 blends showed an improved DI trend of 19-36 percent against the lowest 3-6-1 blends at 6-26 percent. This is confirmed by the correlation analysis of the permeability test results
4. The chloride ion penetration and chloride diffusion coefficient decreased as the CBW content increased from 1 to 4, the alkali concentration decreased from 0 to 2M, and the CSA content decreased from 4 to 1. Its capacity to bind chlorides and alter the concrete microstructure is probably to blame for this effect. (However, the present investigation did not directly evaluate the HAC chloride binding capacity).
5. In comparison to regular Portland cement, 5-1-4 (2 M) holds up better in hotter environments. The harmful expansion that occurs at high temperatures is caused by the limited lime in 5-1-4 blends. Compared to OPC, the 5-1-4 (2 M) system is the superior fire-resistant binder. So, it's clear that CBW-CSA based on alkali activation can be made for building purposes; these materials show much promise for fire resistance.

ACKNOWLEDGMENTS

The authors gratefully acknowledge MAPRONANO ACE, Uganda and the World Bank for the PhD research scholarship. Access to the scholarly repository and library materials at Pwani University, Kenya is appreciated. Thanks to the University of the Witwatersrand, South Africa, and Mombasa Cement Company, Kenya, for allowing access to their cement laboratory. Special thanks to Prof. Luca Valentini of the University of Padova, Italy, for allowing part of the research in their laboratories and for great input and advice in analyzing the results.

ETHICS

There are no ethical issues with the publication of this manuscript.

DATA AVAILABILITY STATEMENT

The authors confirm that the data that supports the findings of this study are available within the article. Raw data that support the finding of this study are available from the corresponding author, upon reasonable request.

CONFLICT OF INTEREST

The authors declare that they have no conflict of interest.

FINANCIAL DISCLOSURE

The authors declared that this study has received no financial support.

USE OF AI FOR WRITING ASSISTANCE

Not declared.

PEER-REVIEW

Externally peer-reviewed.

REFERENCES

[1] Andrew, R. M. (2020). A comparison of estimates of global carbon dioxide emissions from fossil carbon sources. *Earth Syst Sci Data, 12*(2), 1437–1465. [CrossRef]

[2] Amer, I., Kohail, M., El-Feky, M. S., Rashad, A., & Khalaf, M. A. (2021). Characterization of alkali-activated hybrid slag/cement concrete. *Ain Shams Eng J, 12*(1), 135–144. [CrossRef]

[3] Provis, J. L. (2014). Green concrete or red herring? Future of alkali-activated materials. *Adv Appl Ceram, 113*(8), 472–477. [CrossRef]

[4] Rashad, A. M., Bai, Y., Basheer, P. M., Collier, N. C., & Milestone, N. B. (2012). Chemical and mechanical stability of sodium sulfate activated slag after exposure to elevated temperature. *Cem Concr Res, 42*(2), 333–343. [CrossRef]

[5] Bahafid, S., Ghabezloo, S., Duc, M., Faure, P., & Sulem, J. (2017). Effect of the hydration temperature on the microstructure of Class G cement: CSH composition and density. *Cem Concr Res, 95*, 270–281. [CrossRef]

[6] Ma, H., Zhu, H., Yi, C., Fan, J., Chen, H., Xu, X., & Wang, T. (2019). Preparation and reaction mechanism characterization of alkali-activated coal gangue-slag materials. *Materials, 12*(14), 2250. [CrossRef]

[7] Zhang, H. Y., Kodur, V., Wu, B., Cao, L., & Wang, F. (2016). Thermal behavior and mechanical properties of geopolymer mortar after exposure to elevated temperatures. *Constr Build Mater, 109*, 17–24. [CrossRef]

[8] Marie, I. (2017). Thermal conductivity of hybrid recycled aggregate-Rubberized concrete. *Constr Build Mater, 133*, 516–524. [CrossRef]

[9] Ullattil, S. G., & Ramakrishnan, R. M. (2018). Defect-rich brown TiO2-x porous flower aggregates: Selective photocatalytic reversibility for organic dye degradation. *ACS Appl Nano Mater, 1*(8), 4045–4052. [CrossRef]

[10] Real, S., & Bogas, J. A. (2017). Oxygen permeability of structural lightweight aggregate concrete. *Constr Build Mater, 137*, 21–34. [CrossRef]

[11] Davidovits, J., & Sawyer, J. L. (1985). *Early high-strength mineral polymer*. US4509985A.

[12] Kuehl, H. (1908). *Slag cement and process of making the same*. US900939A.

[13] Rivera, J., Castro, F., Fernández-Jiménez, A., & Cristelo, N. (2021). Alkali-activated cements from urban, mining and agro-industrial waste: State-of-the-art and opportunities. *Waste and Biomass Valorization, 12*, 2665–2683. [CrossRef]

[14] Al-Kutti, W., Nasir, M., Johari, M. A. M., Islam, A. S., Manda, A. A., & Blaisi, N. I. (2018). An overview and experimental study on hybrid binders containing date palm ash, fly ash, OPC and activator composites. *Constr Build Mater, 159*, 567–577. [CrossRef]

[15] EAS, K. (2000). Kenya standard test method for determination of cement strength.

[16] Alexander, M. G., Ballim, Y., & Mackechnie J. (2018). Durability index testing procedure manual version 4.5.1. https://tinyurl.com/evkvcakb

[17] Moore, A. J., Bakera, A. T., & Alexander, M. G. (2020). Water sorptivity and porosity testing of concrete. *Concrete Beton Technical Note, 162*, 13–16.

[18] University of Cape Town. (2015). *Concrete durability index testing - Oxygen permeability test*. SANS 3001-CO3-2.

[19] Kenya Bureau of Standards. (2017). *Kenya's standard test method for oxide specification of hydraulic cement*. KS EAS 18-1.

[20] Samson, E., Marchand, J., & Snyder, K. A. (2003). Calculation of ionic diffusion coefficients on the basis of migration test results. *Materials and Structures, 36*, 156–165. [CrossRef]

[21] Castellote, M., Andrade, C., & Alonso, C. (2000). Phenomenological mass-balance-based model of migration tests in stationary conditions: Application to non-steady-state tests. *Cem Concr Res, 30*(12), 1885–1893. [CrossRef]

[22] Crank, J. (1975). *The mathematics of diffusion*. Clarendon Press.

[23] Monteiro, P. J., Geng, G., Marchon, D., Li, J., Alapati, P., Kurtis, K. E., & Qomi, M. J. A. (2019). Advances in characterizing and understanding the microstructure of cementitious materials. *Cem Concr Res, 124*, 105806. [CrossRef]

[24] Abdellatief, M., Elemam, W. E., Alanazi, H., & Tahwia, A. M. (2023). Production and optimization of sustainable cement brick incorporating clay brick wastes using response surface method. *Ceram Int, 49*(6), 9395–9411. [CrossRef]

[25] Assi, L. N., Deaver, E. E., & Ziehl, P. (2018). Effect of source and particle size distribution on the mechanical and microstructural properties of fly Ash-Based geopolymer concrete. *Constr Build Mater, 167*, 372–380. [CrossRef]

[26] Schackow, A., Correia, S. L., & Effting, C. (2020). Microstructural and physical characterization of solid wastes from clay bricks for reuse with cement. *Environ Eng Manag J, 19*(4), 565–576. [CrossRef]

[27] Zhou, H., Chen, Y., Li, H., Xu, Z., Dong, H., & Wang, W. (2022). Effect of particles micro characteristics destroyed by ball milling on fly ash electrostatic separation. *Advanced Powder Technology, 33*(3), 103449. [CrossRef]

[28] Arslan, V. (2021). A study on the dissolution kinetics of iron oxide leaching from clays by oxalic acid. *Physicochemical Problems of Mineral Processing, 57*(3), 97–111. [CrossRef]

[29] Hou, P., Kawashima, S., Kong, D., Corr, D. J., Qian, J., & Shah, S. P. (2013). Modification effects of colloidal nanoSiO2 on cement hydration and its gel property. *Composites Part B Engineering, 45*(1), 440–448. [CrossRef]

[30] Anuar, M. F., Fen, Y. W., Zaid, M. H. M., Matori, K. A., & Khaidir, R. E. M. (2020). The physical and optical studies of crystalline silica derived from the green synthesis of coconut husk ash. *Appl Sci, 10*(6), 2128. [CrossRef]

[31] Tayade, R. A., & Kanojiya, M. A. C. (2022) The case study of isothermal adsorption of phenol, O-cresol on natural charcoal's and applications. *Int J Res Appl Sci Eng Technol, 10*(12), 1718–1731. [CrossRef]

[32] Onwona-Agyeman, B., Lyczko, N., Minh, D. P., Nzihou, A., & Yaya, A. (2020). Characterization of some selected Ghanaian clay minerals for potential industrial applications. *J Ceram Process Res, 21*(1), 35–41. [CrossRef]

[33] de Sousa, L. L., Salomão, R., & Arantes, V. L. (2017). Development and characterization of porous moldable refractory structures of the alumina-mullite-quartz system. *Ceram Int, 43*(1), 1362–1370. [CrossRef]

[34] Garg, N., & Skibsted, J. (2016). Pozzolanic reactivity of a calcined interstratified illite/smectite (70/30) clay. *Cem Concr Res, 79*, 101–111. [CrossRef]

[35] Kang, S. H., Hong, S. G., & Moon, J. (2019). The use of rice husk ash as reactive filler in ultra-high performance concrete. *Cem Concr Res, 115*, 389–400. [CrossRef]

[36] Opálková Šišková, A., Dvorák, T., Šimonová Baranyaiová, T., Šimon, E., Eckstein Andicsová, A., Švajdlenková, H., ... & Nosko, M. (2020). Simple and eco-friendly route from agro-food waste to water pollutants removal. *Materials, 13*(23), 5424. [CrossRef]

[37] Park, S., Baker, J. O., Himmel, M. E., Parilla, P. A., & Johnson, D. K. (2010). Cellulose crystallinity index: Measurement techniques and their impact on interpreting cellulase performance. *Biotechnol Biofuels, 3*, 1–10. [CrossRef]

[38] Scrivener, K. L., & Nonat, A. (2011). Hydration of cementitious materials, present and future. *Cem Concr Res, 41*(7), 651–665. [CrossRef]

[39] Khushnood, R. A. O. & Arsalan, R. (2015). *High performance self-compacting cementitious materials using nano/micro carbonaceous inerts* [Doctoral thesis], Politecnico di Torino.

[40] Barboza-Chavez, A. C., Gómez-Zamorano, L. Y., & Acevedo-Dávila, J. L. (2020). Synthesis and characterization of a hybrid cement based on fly ash, metakaolin and portland cement clinker. *Materials, 13*(5), 1084. [CrossRef]

[41] Samarakoon, M. H., Ranjith, P. G., Rathnaweera, T. D., & Perera, M. S. A. (2019). Recent advances in alkaline cement binders: A review. *J Clean Prod, 227*, 70–87. [CrossRef]

[42] Musyimi, N.F., Karanja, T.J., Wachira, M.J., & Mulwa, M.O. (2016). Pozzolanicity and compressive strength performance of kibwezi bricks based cement. *IOSR J Appl Chem, 9*(2), 28–32.

[43] Hanein, T., Thienel, K. C., Zunino, F., Marsh, A. T., Maier, M., Wang, B., ... & Martirena-Hernandez, F. (2022). Clay calcination technology: State-of-the-art review by the RILEM TC 282-CCL. *Mater Struct, 55*(1), 3. [CrossRef]

[44] Chernyshova, N., Lesovik, V., Fediuk, R., & Timokhin, R. (2020). Enhancement of fresh properties and performances of the eco-friendly gypsum-cement composite (EGCC). *Constr Build Mater, 260*, 120462. [CrossRef]

[45] Bakera, A. T., & Alexander, M. G. (2018). *Properties of Western Cape concretes with metakaolin*. In MATEC Web of Conferences (Vol. 199, p. 11011). EDP Sciences. [CrossRef]

[46] Kearsley, E. P., & Wainwright, P. J. (2001). Porosity and permeability of foamed concrete. *Cem Concr Res, 31*(5), 805–812. [CrossRef]

[47] Marangu, J. M., Thiong'o, J. K., & Wachira, J. M. (2019). Review of carbonation resistance in hydrated cement based materials. *J Chem, 2019*(1), 8489671. [CrossRef]

[48] Cordeiro, G. C., Toledo Filho, R. D., Tavares, L. M., & Fairbairn, E. D. M. R. (2009). Ultrafine grinding of sugar cane bagasse ash for application as pozzolanic admixture in concrete. *Cem Concr Res, 39*(2), 110–115. [CrossRef]

[49] van Deventer, J. S., San Nicolas, R., Ismail, I., Bernal, S. A., Brice, D. G., & Provis, J. L. (2015). Microstructure and durability of alkali-activated materials as key parameters for standardization. *J Sustain Cem Mater, 4*(2), 116–128. [CrossRef]

[50] Nath, P., & Sarker, P. K. (2014). Effect of GGBFS on setting, workability and early strength properties of fly ash geopolymer concrete cured in ambient condition. *Constr Build Mater, 66*, 163–171. [CrossRef]

[51] Fang, S., Lam, E. S. S., Li, B., & Wu, B. (2020). Effect of alkali contents, moduli and curing time on engineering properties of alkali activated slag. *Constr Build Mater, 249*, 118799. [CrossRef]

[52] Monticelli, C., Natali, M. E., Balbo, A., Chiavari, C., Zanotto, F., Manzi, S., & Bignozzi, M. C. (2016). Corrosion behavior of steel in alkali-activated fly ash mortars in the light of their microstructural, mechanical and chemical characterization. *Cem Concr Res, 80*, 60–68. [CrossRef]

[53] Palomo, A., Krivenko, P., Garcia-Lodeiro, I., Kavalerova, E., Maltseva, O., & Fernández-Jiménez, A. (2014). A review on alkaline activation: New analytical perspectives. *Mater Constr, 64*(315), e022. [CrossRef]

[54] Angulo-Ramírez, D. E., Valencia-Saavedra, W. G., & Mejía de Gutiérrez, R. (2020). Alkali-activated concretes based on fly ash and blast furnace slag: Compressive strength, water absorption and chloride permeability. *Ing Investig, 40*(2), 72–80. [CrossRef]

[55] Puertas, F., Palacios, M., Manzano, H., Dolado, J. S., Rico, A., & Rodríguez, J. (2011). A model for the CASH gel formed in alkali-activated slag cements. *J Eur Ceram Soc, 31*(12), 2043–2056. [CrossRef]

[56] Embong, R., Kusbiantoro, A., Shafiq, N., & Nuruddin, M. F. (2016). Strength and microstructural properties of fly ash based geopolymer concrete containing high-calcium and water-absorptive aggregate. *J Clean Prod, 112*, 816–822. [CrossRef]

[57] Gijbels, K., Pontikes, Y., Samyn, P., Schreurs, S., & Schroeyers, W. (2020). Effect of NaOH content on hydration, mineralogy, porosity and strength in alkali/sulfate-activated binders from ground granulated blast furnace slag and phosphogypsum. *Cem Concr Res, 132*, 106054. [CrossRef]

[58] Verma, P., Chowdhury, R., & Chakrabarti, A. (2021). Role of graphene-based materials (GO) in improving physicochemical properties of cementitious nano-composites: A review. *J Mater Sci, 56*(35), 19329–19358. [CrossRef]

[59] Balun, B., & Karataş, M. (2021). Influence of curing conditions on pumice-based alkali activated composites incorporating Portland cement. *J Build Eng, 43*, 102605. [CrossRef]

[60] Bernal, S. A., San Nicolas, R., Myers, R. J., de Gutiérrez, R. M., Puertas, F., van Deventer, J. S., & Provis, J. L. (2014). MgO content of slag controls phase evolution and structural changes induced by accelerated carbonation in alkali-activated binders. *Cem Concr Res, 57*, 33–43. [CrossRef]

[61] Mithun, B. M., & Narasimhan, M. C. (2016). Performance of alkali activated slag concrete mixes incorporating copper slag as fine aggregate. *J Clean Prod, 112*, 837–844. [CrossRef]

[62] Yang, K., Yang, C., Magee, B., Nanukuttan, S., & Ye, J. (2016). Establishment of a preconditioning regime for air permeability and sorptivity of alkali-activated slag concrete. *Cem Concr Res, 73*, 19–28. [CrossRef]

[63] Albitar, M., Ali, M. M., Visintin, P., & Drechsler, M. (2017). Durability evaluation of geopolymer and conventional concretes. *Constr Build Mater, 136*, 374–385. [CrossRef]

[64] Ismail, I., Bernal, S. A., Provis, J. L., San Nicolas, R., Hamdan, S., & van Deventer, J. S. (2014). Modification of phase evolution in alkali-activated blast furnace slag by the incorporation of fly ash. *Cem Concr Compos, 45*, 125–135. [CrossRef]

[65] Ngui Musyimi, F., Wachira, J. M., Thiong'o, J. K., & Marangu, J. M. (2019). Performance of ground clay brick mortars in simulated chloride and sulphate media. *J Eng, 2019*(1), 6430868. [CrossRef]

[66] Mutitu, D. K., Karanja, J. K., Wachira, J. M. (2014). Diffusivity of chloride and sulphate ions into mortar cubes made using ordinary Portland and Portland Pozzolana cements. *IOSR J Appl Chem, 7*(2), 67–73. [CrossRef]

[67] Wang, J., Basheer, P. M., Nanukuttan, S. V., & Bai, Y. (2014). *Influence of compressive loading on chloride ingress through concrete*. In Civil Engineering Research Association of Ireland (CERAI) Proceedings. CERI 2014, Spain.

[68] Marangu, J. M., Thiong'o, J. K., & Wachira, J. M. (2018). Chloride ingress in chemically activated calcined clay-based cement. *J Chem, 2018*(1), 1595230. [CrossRef]

[69] Tang, S., Wang, Y., Geng, Z., Xu, X., Yu, W., & Chen, J. (2021). Structure, fractality, mechanics and durability of calcium silicate hydrates. *Fractal and Fractional, 5*(2), 47. [CrossRef]

[70] Zhang, H., He, B., Zhao, B., & Monteiro, P. J. (2023). Using diatomite as a partial replacement of cement for improving the performance of recycled aggregate concrete (RAC)-Effects and mechanism. *Constr Build Mater, 385*, 131518. [CrossRef]

[71] Juenger, M. C., & Siddique, R. (2015). Recent advances in understanding the role of supplementary cementitious materials in concrete. *Cem Concr Res, 78*, 71–80. [CrossRef]

[72] Abdulkareem, O. M., Fraj, A. B., Bouasker, M., Khouchaf, L., & Khelidj, A. (2021). Microstructural investigation of slag-blended UHPC: The effects of slag content and chemical/thermal activation. *Constr Build Mater, 292*, 123455. [CrossRef]

[73] Živica, V., Palou, M. T., & Križma, M. (2015). Geopolymer cements and their properties: A review. *Build Res J, 61*(2), 85–100. [CrossRef]

[74] Zhang, Z., Provis, J. L., Reid, A., & Wang, H. (2014). Geopolymer foam concrete: An emerging material for sustainable construction. *Constr Build Mater, 56*, 113–127. [CrossRef]

[75] Lin, W., Zhou, F., Luo, W., & You, L. (2021). Recycling the waste dolomite powder with excellent consolidation properties: Sample synthesis, mechanical evaluation, and consolidation mechanism analysis. *Constr Build Mater, 290*, 123198. [CrossRef]

[76] Jeon, D., Yum, W. S., Song, H., Sim, S., & Oh, J. E. (2018). The temperature-dependent action of sugar in the retardation and strength improvement of Ca (OH) 2-Na2CO3-activated fly ash systems through calcium complexation. *Constr Build Mater, 190*, 918–928. [CrossRef]

[77] Rashad, A. M. (2015). Influence of different additives on the properties of sodium sulfate activated slag. *Constr Build Mater, 79*, 379-389. [CrossRef]